Numerical Simulation of Mutual Capacitance Touch Screens for Ungrounded Objects

Christian Bjørge Thoresen and Ulrik Hanke, *Senior Member, IEEE*

***Abstract*—Mutual capacitance touch screens translate billions of finger touches to digital signals around the world daily. By enabling these screens to detect ungrounded objects, it may be possible to extend their functionality by detecting tangible user interface objects on the screen surface. This article presents results from finite element method simulations, as well as experiments, showing that the mutual capacitance touch screen panel sensing principle can be used to detect ungrounded objects. Looking into how different design parameters of the touch panel affect grounded and ungrounded touch differently, we have found a film-glass-film stack-up to be 1.55 times more sensitive to ungrounded than grounded touch, compared to 0.65 and 0.20 for two different configurations of glass-film stack-up.**

***Index Terms*—capacitive sensing, tangible user interface.**

I. Introduction

In RECENT years, touch screens have become one of the most common human computer interfaces. Touch screens offer a direct and intuitive interaction with the information displayed on the screen, as well as being space saving and independent of external input devices. However, they do not offer the haptic feedback of traditional user interfaces, such as buttons, keyboards, control knobs and levers. With Tangible User Interface (TUI) for touch screens, the interaction happens through manipulation of physical objects on the screen. This is one possible way of bringing haptic feedback to touch screens. Such an interface has been demonstrated for rear camera based optical touch screens [1], [2]. These screens are susceptible to interference from ambient light. It is therefore of interest to look into designing TUI for other touch screen technologies.

In the consumer market, mutual capacitance touch screen panels [3] (TSPs) have become the most applied touch screen technology. They are found in nearly all smart phones and tablets. This technology offers true multi-touch detection and compared to resistive touch screens, no physical force is required to trigger touches. Commercially available TSP devices are designed for detecting human fingers. Previous work has described TUI design for TSPs based on mimicking fingers using electric conductors in contact with the hand of the operator [4]. This range from simple folded paper designs [5] to 3D-printed tangibles [6]. Tangible identification may be done either by a spatial pattern of touches or by toggling a touch point on and off by a circuit in the tangible [7].

This work was supported by The Research Council of Norway, NFR project no 217788.

Christian Bjørge Thoresen and Ulrik Hanke were with respectively the Departement of Maritime Operations and the Department of Microsystems at the University College of Southeast Norway, Campus Vestfold, Raveien 215, NO-3184 Borre, Norway

Limitations of these designs include inability of the TSP to detect an untouched tangible, rejection of static touches by TSP filtering algorithms and a large area required for identification patterns. These limitations are all a result of the need to mimic finger touches. We therefore seek to find out whether different TSP designs or algorithms can be used to overcome or reduce these limitations. In this paper we focus in particular on the possibility of detecting untouched tangibles. Possible applications of this is for instance operating the TUI with electrically insulating gloves or detection of the position of physical board game pieces on a game board displayed on the screen.

To determine if changing the TSP design or algorithms could benefit TUI design, we need to take a closer look at the working principle of TSPs. In general they work by measuring the mutual capacitance between two sets of electrodes. These sets are typically oriented in vertical and horizontal direction across the screen. Considering a measurement principle where a signal is applied to one electrode in one set and picked up by the electrodes in the other set, we refer to the electrodes in these sets respectively as Tx- and Rx-electrodes. By iterating through all the combinations of Tx- and Rx-electrodes, the TSP controller builds an image of the measured mutual capacitance (C_m) for each electrode intersection.

C_m is influenced by conductive or dielectric materials in close proximity to the electrode intersection. Fig. 1 shows a simplified illustration of how the electric field set up by the active Tx-electrode is influenced by a conductive pad on the screen surface. The case shown for a grounded pad is similar to regular touch by a human finger, where the capacitive coupling from finger to signal ground in the TSP is relatively strong. In this case, the pad disrupts the electric field between the Tx- and Rx-electrode, causing a reduction of C_m. We denote the change in mutual capacitance as ΔC_m.

In the other case of an ungrounded pad, the capacitive coupling from pad to signal ground is weak. In that case, the pad acts as a bridge for the electric field, leading to an increase in C_m. For these two cases we have only considered the extremes of no capacitive coupling or direct coupling to ground. In reality, pads can have different levels of ground coupling other than these extremes, leading to different degrees of increase or reduction of C_m.

Regular commercial TSP controllers are designed to detect finger touches. They report areas of negative ΔC_m corresponding to that of a finger as a touch. Some controllers may also report touch size and finger direction. Filter algorithms are used to reject other kinds of touch, for instance palm rejection, and also to compensate for drift in C_m by updating

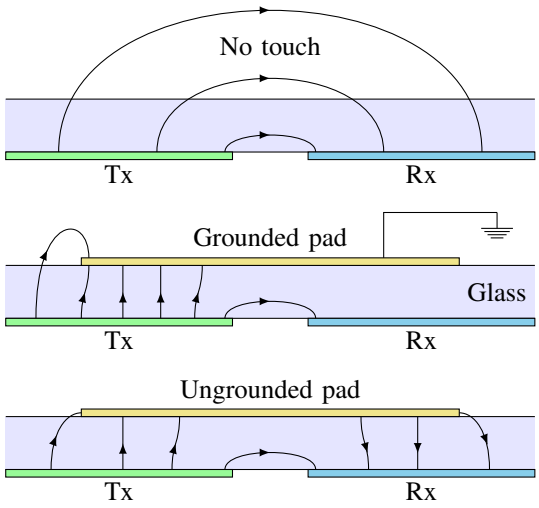

Fig. 1. Cross-section illustration of the working principle for a mutual capacitance TSP, showing how the electric field is changing for the different conditions of no-touch, grounded pad touch and ungrounded pad touch. Electrodes are shown as coplanar and the effect of glass permittivity is ignored for simplicity.

the reference value for C_{m} used to calculate ΔC_{m}. A TUI design based on mimicking regular touch, where the algorithm simply processes the touch events reported by a regular TSP controller, is therefore subject to the limitations of not processing the capacitance image directly. Ungrounded pads can not be detected, static touches may be filtered out and the TUI identification pattern is limited to using the spatial distribution of a number of touch events, possibly including touch size and orientation depending on the level of detail of the touch events reported by the TSP controller.

A previously described method of using ground coupling through the TSP itself for detection of untouched tangibles [8] is also affected severely by these limitations. This method requires larger area for the tangible, as it impose further restrictions on the possible spatial identification patterns. It is also more sensitive to the filtering of static touches due to the weak touch signals it generates. Another possible option for untouched TUI detection is the use of a tether wire connecting the TUI object to signal ground. Such a wire may be inconvenient in several ways. The thick insulation required to prevent unwanted touch events will obstruct view of the screen, and the wire itself will interfere with the operations of the rest of the TSP. Multiple tangibles may lead to entangled tethers.

The actual processing of TSP capacitance images is not well documented in literature. Rekimoto gives an early description of the mutual capacitance TSP principle in [4], including capacitance images for different touch input and the concept of an operator grounded TUI object. Holz et al. demonstrate how the capacitance image of the user's ear can be used for identification on a smart phone device [9]. However, neither of these depicts the effect of putting ungrounded objects on the screen. For considering the possibility of designing TUI objects with ungrounded pads, knowledge of how they are seen by the TSP is necessary. In this article we therefore look into simulating how variations in the design of the TSP influence the capacitance images for grounded and ungrounded pads differently. With access to TSP capacitance images from one specific TSP device, we compare simulated and experimental capacitance images for a set of ungrounded and grounded pads. Customized processing of the capacitance image could also open up for the use of the TSP for other capacitive sensing applications[10]. 3D printed capacitive sensor structures, as described in [11], could possibly work directly with the TSP, with no need of embedded electronics.

Whereas a typical TUI application would require several pads in a pattern for identification, we have for this article chosen to look at only one single ungrounded or grounded pad on the TSP, as shown in Fig. 2 and Fig. 4. A comparison of the ungrounded versus grounded touch images gives a starting point for understanding the considerations to make for analyzing the case of multiple pads. Also the finite element method (FEM) used for simulation limits the TSP area that can be simulated, and simulating a full TUI multi-pad pattern would require significantly more time and computational resources.

Mutual capacitive TSPs can have several different electrode layouts. We have chosen to look at the Manhattan configuration, where the electrodes consist of orthogonal strips in two layers, as illustrated in Fig. 2. For this design, the overlapping area of the Rx- and Tx-electrodes contributes most of C_{m}. The capacitance from this region is not affected by the presence of objects on the screen, as the Rx-electrode is shielding it from the surface of the screen. For modeling only ΔC_{m} for different kind of touch input, we have therefore previously looked into a model where both Rx- and Tx-electrodes are in the same plane, but where the Tx-electrodes have been cut to leave room for the top Rx-electrodes [12]. This leads to a model that is less computationally demanding than a full model, and where mesh convergence for a 5 by 5 electrode simulation can be achieved with about 4 GB of memory. This model was sufficiently accurate to qualitatively show the effect of ungrounded touch. However, we have found that especially the mutual capacitance for ungrounded touch is sensitive to the width of the artificial horizontal gap between Tx- and Rx-electrode. For the continued work presented here, we have therefore used full models.

In this article, we present and compare the results of varying the TSP parameters for three different configurations of the Manhattan layout. The parameters we have looked at are relative permittivity and thickness of the glass and the polymer film, Rx-electrode width, electrode pitch, pad radius and gap between pad and screen. The layer structure or stack-ups of the configurations are shown in Fig. 3 and the electrode layouts are shown in Fig. 4, with symbol names for all dimension parameters. Configuration (A) is the regular glass-film stack-up, where the Rx- and Tx-electrodes are on opposite sides of a polymer film bonded to the bottom side of the glass panel. Configuration (B) has the same stack-up, but each Rx-electrode consists of two strips connected in parallel instead of one. In this case we let the Rx-width parameter denote the total width of the two strips in each pair, so the individual strip width is half of that in configuration (A). Configuration

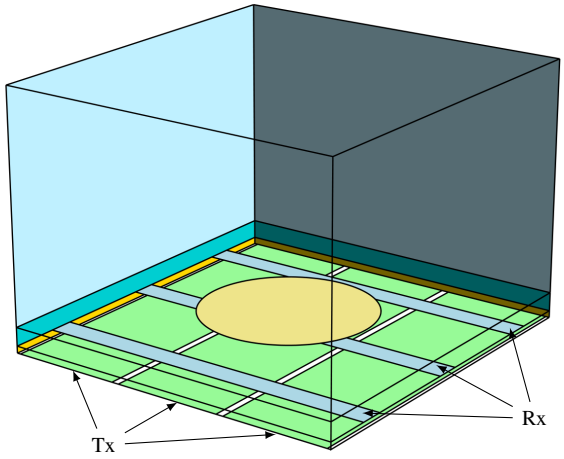

Fig. 2. 3D model of the simulation volume used for 3 by 3 electrodes in configuration (a), with a circular conductive pad on the glass surface. The interfaces are fully transparent.

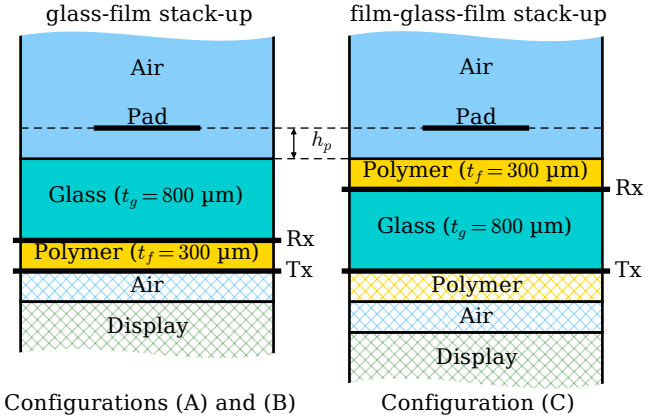

Fig. 3. TSP stack-ups for the three configurations. The region below the Tx-electrode layer is not included in the FEM models.

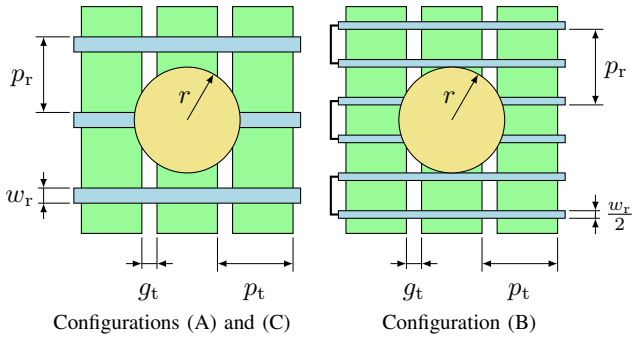

Fig. 4. Top-down view of the different electrode configurations, showing our definitions of lateral dimension parameters.

(C) has a film-glass-film stack-up with the Rx-electrodes and Tx-electrodes on opposite sides of the glass.

These configurations stem from actual devices. Configuration (A) is from the original TSP in a Samsung Galaxy Note 10.1 (GT-N8010), as used in the experiments in section III.

TABLE I
DEFAULT SIMULATION PARAMETERS

Parameter	Symbol	Value	Unit
Glass thickness	t_g	0.8	mm
Film thickness	t_f	0.3	mm
Tx-electrode pitch	p_t	5.09	mm
Rx-electrode pitch	p_r	5.27	mm
Tx-electrode gap	g_t	0.32	mm
Rx-electrode width	w_r	1.07	mm
Relative permittivity of glass	ε_g	7.0	
Relative permittivity of polymer film	ε_f	3.5	
Pad radius	r	5.0	mm
Pad to screen gap	h_p	0	mm

Configuration (B) is from a replacement TSP for the same device. The parameter values we used as default parameters for simulations, listed in Table I, are based on the GT-N8010. The difference in pitch for Tx-electrode and Rx-electrode stems from this device. Lateral dimensions were found using optical microscopy of the original TSP. The glass and film thickness were measured physically in the replacement TSP, using a caliper. The values used for relative permittivities are based on typical values seen for toughened touchscreen glass [13] and for polyethylene terephthalate (PET). We have been able to extract debug data from the TSP controller in the GT-N8010 TSP device, allowing us to compare the simulation results with experimental data. The film-glass-film stack-up of configuration (C), illustrated in Fig. 3, was seen in a TSP for a device called ONDA VX610W 7".

Several possible circuit principles exist for mutual capacitance touch controllers. We will in general consider designs that keep the Rx-electrodes at virtual ground. This would typically be the case for designs featuring charge amplifier or charge integrator circuits as front ends. The oscillator design described in [14] does not fall within this category, nor does designs using a voltage amplifier as front end.

Whereas the electrode signals in a TSP are time-varying and therefore influenced by the series resistance of the electrodes and wiring, for a charge transfer circuit, the output signals are held constant long enough for the input to settle. We will therefore model the charge transfer using an electrostatic model.

The remainder of this paper is organized as follows: Section II presents the details of the FEM model setup. Section III presents the gathering of experimental data from the GT-N8010 tablet. Section IV presents the results of the FEM simulations and comparison between FEM simulations and experimental data. Finally, our suggestions for future work and our conclusion is presented in sections V and VI.

II. FEM SIMULATIONS

We used the open source multiphysical simulation software Elmer (v 8.2) [15] for electrostatic FEM, paired with Gmsh (2.12.0) [16] for geometry and mesh generation (on 64-bit Linux). Python scripting was used for performing automatic parameter sweeps and post-processing of results.

A. FEM Setup Verification

A 3D simulation of the capacitance between two coplanar, zero-thickness conductive strips in free space was used to verify the FEM setup. This problem is related to that of simulating a TSP featuring strip electrodes. We used a strip width $s = 5\,\mathrm{mm}$, a strip length of $l = 5\,\mathrm{mm}$ and a gap between the strips of $g = 1\,\mathrm{mm}$ in free air. These dimensions are in the same order of magnitude as those found in a TSP. An analytic expression for the capacitance can be found using conformal mapping, and based on the derivations in [17], we get the capacitance as

$$C = \varepsilon_0 l \frac{K(k_0')}{K(k_0)}, \tag{1}$$

where $k_0 = g/(s+g)$, $k_0' = \sqrt{1-k_0^2}$ and $K(k)$ is the elliptic integral of the first kind. Inserting our values yields $107\,\mathrm{fF}$.

For the FEM model, the strips were contained in a box shaped volume of width and height $4\,\mathrm{cm}$ and depth equal to the length of the strips, l. All the outer boundaries were set to no electric field flux condition.

Gmsh will by default generate a free tetrahedral mesh, where the characteristic element length can be specified at each point defining the geometry. This can be used to refine the mesh close to the edges of the electrodes and the pad. However it will not affect the mesh of neighboring surfaces, only the volume. In order for the TSP model to also have refinement in the surface mesh of both pad and electrodes, we used the boundary layer field to control the mesh refinement along the strip edges. For a mesh with 380 000 elements and refinement along the gap facing edge of the strips, the simulated capacitance is $1.1\,\%$ higher than the analytical capacitance. A mesh of the same domain, having uniform density, with 5 million elements shows an error of $3.5\,\%$. This indicates that the mesh refinement used helps in achieving more accurate results using less computational resources.

B. TSP Model

For the TSP, we have looked at the Manhattan configuration with orthogonal intersecting strip line electrodes. With design of tags for tangible user interface in mind, we model the mutual capacitances resulting from a conductive circular pad on the screen. As an electrostatic FEM simulation of a complete touch screen panel would require a large amount of computational resources and time, we limit our model to 3 by 3 or 5 by 5 electrodes depending on the electrode pitch and the size and displacement of the pad. For an electrode pitch of $5\,\mathrm{mm}$ and a centered pad of radius $5\,\mathrm{mm}$, we have a margin of $2.5\,\mathrm{mm}$ from the edge of the pad to the edge of the simulation volume for a 3 by 3 electrodes simulation. For smaller pitch, larger pad radius or displacement of the pad, we have used 5 by 5 electrodes simulations. Except for the simulations of varying pad displacement, we report the results for the center electrode intersection under a centered pad.

In our simulation, we have used a height of the air volume above the screen of $1\,\mathrm{cm}$. We found that variation of the air volume thickness did not significantly influence the results until it was reduced below $3\,\mathrm{mm}$. As we only consider the mutual capacitance between the electrodes, we have not included the volume below the Tx-electrodes in our model. This region is of interest when analyzing noise performance of the TSP, where capacitive coupling to the display matters. When the gaps between the Tx-electrodes are small, the fringe field passing through from the bottom side of the Tx-electrodes will be small compared to the field from the top side, and thus have little influence on the mutual capacitances between Tx- and Rx-electrodes. For TSPs, the electrode thickness is in the order of $100\,\mathrm{nm}$ or less, so the zero-thickness approximation used for coplanar strips in the FEM verification is also applied to the TSP electrodes.

C. Capacitance Calculations

We used the capacitance matrix function of the electrostatic solver in Elmer to calculate the mutual capacitances. The function automatically runs a simulation for each capacitance body specified in the boundary conditions, where it applies a voltage to that body and calculates the resulting charge on the remaining bodies as the sum of charges on the mesh nodes belonging to each capacitance body. The output is a capacitance matrix with the mutual capacitances between each body.

We specified each electrode and the pad to be independent capacitance bodies. The mutual capacitance, C_m, under the condition of grounded pad, denoted C_m', is then given directly by the capacitance matrix. For grounded touch, we denote the change in capacitance as $\Delta C_\mathrm{m}' = C_\mathrm{m}' - C_\mathrm{m}$.

By assuming the pad to be a floating conductor, the effective mutual capacitance between electrodes for the ungrounded case can be determined as follows: Let C_t be the capacitance between the pad and the active Tx-electrode. We assume all the other electrodes to be held at ground potential and let C_g be the total capacitance between the pad and these electrodes. With a voltage V_t applied to the active Tx-electrode, the voltage of the pad is given by a capacitive voltage divider as

$$V_\mathrm{p} = \frac{C_\mathrm{t}}{C_\mathrm{t} + C_\mathrm{g}} V_\mathrm{t}. \tag{2}$$

Now, with C_r as the capacitance between the pad and the active Rx-electrode, the charge on that electrode is given by

$$Q_\mathrm{r} = V_\mathrm{p} C_\mathrm{r}. \tag{3}$$

Finally the effective mutual capacitance between the active Tx-electrode and the chosen Rx-electrode under the condition of ungrounded touch is given as

$$C_\mathrm{m}^* = \frac{Q_\mathrm{r}}{V_\mathrm{t}} = \frac{C_\mathrm{r} C_\mathrm{t}}{C_\mathrm{t} + C_\mathrm{g}}. \tag{4}$$

We let $\Delta C_\mathrm{m}^* = C_\mathrm{m}^* - C_\mathrm{m}$ denote the capacitance change for ungrounded touch. Calculating the capacitance using (4) on the capacitance matrix gives the same result as running the simulation with a floating potential boundary condition for the pad. With a total of n Tx- and Rx-electrodes, we need $n+1$ simulation runs, compared to $2n$ if we had used the floating potential boundary condition for the pad. As the Tx to Tx elements are not needed, simulation time could have

TABLE II
MESH CONVERGENCE: % CHANGE IN $\Delta C'_{\mathrm{m}}$

	Configurations		
Element size (μm)	**(A)**	**(B)**	**(C)**
1000			
500	−48	−41	−1.9
250	−33	−20	14
125	−14	−10	2.8
62.5	3.1	5.8	3
31.2	−2.5	0.28	−0.65
15.6	0.69	1.6	−0.03

TABLE III
SIMULATION RESOURCES

	Solver		Mesh
Model	**Memory (GB)**	**Time[a](s)**	**Time[b](s)**
3x3 (a,c)	3.7	83	69
3x3 (b)	5.0	130	94
5x5 (a,c)	8.5	350	170
5x5 (b)	12	440	260

[a] Using 12 parallel threads.
[b] Average for parallel mesh generation on multiple cores.

been reduced further by modifying the solver to skip the Tx-electrode permutation leading to $n_{\mathrm{t}} + 1$ simulations for n_{t} Tx-electrodes.

D. Mesh Convergence And Resource Usage

We performed mesh convergence analysis for each of the electrode configuration models. Using 5 by 5 electrode simulations, we divided the smallest element size in two for subsequent simulations. The resulting changes in $\Delta C'_{\mathrm{m}}$ are shown in Table II. For the two finest element sizes listed, the change is $2.5\,\%$ or less. We considered the element size setting of $15\,\mu\mathrm{m}$ to provide sufficient mesh convergence and have used this setting for further simulations.

Average resource usages for the different models are listed in Table III. The simulations were run on a 6-core Intel i7-5820K system with 64 GB memory, supporting 12 threads in parallel. For efficient use of the computing resources, we therefore executed Elmer using OpenMPI, with 12 instances. Since Gmsh does not support multihtreading, but require less memory than the solver, we ran Gmsh for several meshes in parallel.

As one more verification of our Elmer and Gmsh setup, we compared the results for a 3x3 model of configuration (a) with results from the same model simulated in COMSOL Multiphysics 5.0. For this simulation, we used an adaptive mesh with 21 million tetrahedral elements. Simulation time excluding meshing was a total of $4550\,\mathrm{s}$ for the seven simulations needed to make the full capacitance matrix. For the COMSOL simulation, we also determined the mutual capacitance of the middle intersection for ungrounded case directly, using the floating potential boundary condition for the pad. The resulting capacitance was equal to the one calculated using (4). The results for default parameters for configuration (a) in COMSOL and for all three configurations in Elmer are listed in Table IV.

TABLE IV
RESULTS FOR DEFAULT PARAMETERS

	COMSOL	Elmer		
Configuration	**(A)**	**(A)**	**(B)**	**(C)**
C_m (pF)	1.06	1.06	1.42	0.82
$\Delta C'_m$ (pF)	−0.26	−0.26	−0.36	−0.21
ΔC^*_m (pF)	0.15	0.17	0.07	0.32
$\lvert\Delta C^*_{\mathrm{m}}/\Delta C'_{\mathrm{m}}\rvert$	0.57	0.65	0.20	1.55

E. Parameter Sweeps

We simulated C_{m}, $\Delta C'_{\mathrm{m}}$ and ΔC^*_{m} resulting from varying the following parameters one by one: The Rx-electrode width, the thickness and relative permittivity of both the glass and the polymer film, the electrode pitch, the pad radius and the gap between pad and the TSP. Default values are listed in Table I. For the electrode pitch sweep, we set $p_{\mathrm{t}} = p_{\mathrm{r}}$, and varied these as one parameter. For the Rx-electrode width sweep, the pitch was kept constant.

F. Pad Displacement

We studied the result of displacing the center of the pad away from the active electrode intersection for independent displacement in both x- and y-direction. Using a displacement step size of $1/16$ pitch, we got 40 by 40 points of data for displacements up to $5/2$ pitches. Utilizing the symmetry of the pad and the results from all 10 electrodes in 5 by 5 simulations, 64 simulations were needed to obtain the 1600 data points. To see how pad radius and configuration influence grounded and ungrounded touch differently, we simulated the results of three different pad radii on each of the three configurations.

III. TOUCH DATA FROM EXPERIMENTS

The tablet device Samsung Galaxy Note 10.1 (GT-N8010) features an Atmel maXTouch mxt1664S controller, which is compatible with the *mxt-app* open source command line utility provided by Atmel. Executing mxt-app as root on the device (with command line argument: -d "i2c-dev:3-004a") gives access to the debug features of the touch controller, including the matrices of capacitance reference levels and capacitance changes, typically called *deltas*. Operating the mxt-app in bridge mode, this data can be transfered by network to a computer for further processing.

The device calculates capacitance deltas as the difference between measurement and reference level. As the reference levels are updated according to an unknown algorithm, to obtain one sample from the device we extract both references and deltas and use the sum of the two. We use this method to first acquire our own reference levels when the screen is untouched and subtract this from subsequent measurements for various touch conditions. Although oscilloscope measurements show that the controller scans the screen at a rate of about

Fig. 5. Back sides of pads made from aluminum tape wrapped around to the backside of cardboard discs, with total thickness of 0.65 mm. The front sides are covered by one layer of aluminum tape. The ruler scale is in cm.

90 Hz, the refresh rate achieved for transferring two sets of data was about 1 Hz. It should also be noted that data is transferred as pages, meaning that one full frame does not represent the data from one single scan cycle, but rather a combination of data from several scan cycles. This is similar to the screen tearing artifact for video displays. The received data is also occasionally corrupted, so this debug data channel is not suitable for any practical application. The slow transfer means that there is a chance that the reference level is updated during acquisition, introducing a small error.

We used the circular pads shown in Fig. 5 to generate data from grounded and ungrounded touches. Each pad was carefully centered above an electrode intersection in the digitizer by means of observing the output image and shifting the pad to obtain symmetry in both x- and y-direction about one center pixel. As the readings from the device may depend on the grounding conditions of the device, we conducted the measurements with the device connected by the USB-cable to a computer connected to a grounded power outlet. For the grounded case of two smaller pads, we used a M4 x 20 mm bolt with a hex nut at the end to press down on the pad, as touching it directly with a finger would affect the fringe field to the back of the pad considerably. For the largest pad, we used a 1 mm thick washer with outer diameter 15 mm to distribute the pressure on the pad, and pressed down on the washer directly with a finger. In both cases the grounding was achieved by touch from a human body.

IV. Results and Discussion

From the simulation results listed in Table IV, we see that there is a difference between the configurations in the sensitivity to grounded versus ungrounded touch. For configuration (A) the ΔC_m for ungrounded touch is 0.65 of the ΔC_m for grounded touch. For configuration (B) this number is as low as 0.20. Configuration (C) has a higher sensitivity to ungrounded touch, with a number of 1.55. For regular finger sensing, favoring grounded touch can help improve immunity against disturbances caused by water droplets or other dielectric or conductive substances. For our use in detecting ungrounded objects, configuration (C) might be worth considering. The exposed polymer film surface makes this design less scratch resistant than the two others. This will not be as much of a disadvantage in an application where the only interaction with

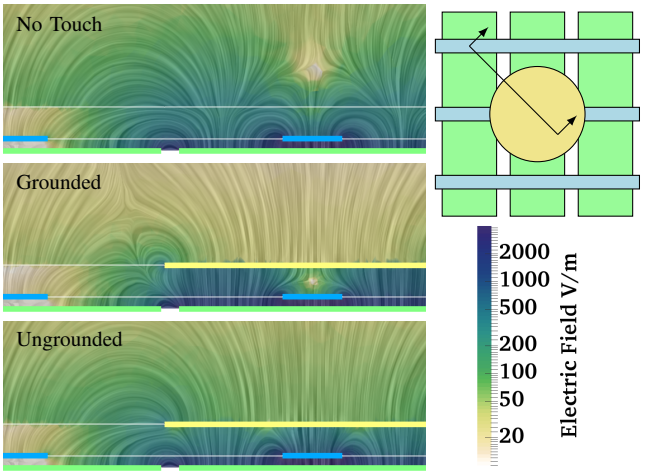

Fig. 6. Simulated electrostatic field for the shown cross-section of electrode configuration (A) under different touch conditions. The field orientation in the cross section plane is illustrated by the Line Integral Convolution method [18]. The thick lines shows the location of the electrodes and the pad. Field strength is for 1 V applied to the middle Tx-electrode.

the screen is through tangibles fitted in slots in a transparent plate covering the screen. Furthermore, the top polymer film might be exchanged with or protected by an ultra thin glass sheet for improved scratch resistance.

Fig. 6 shows the electrical field simulated for the three different touch conditions. This figure supports the simplified illustration in Fig. 1. Looking at the region between the rightmost Rx-electrode and the pad, we see how a grounded pad is disrupting the field and an ungrounded pad is bridging it, respectively giving rise to a negative and positive change in C_m.

A. Parameter Sweep

The results of the parameter sweeps in Fig. 7 show how the TSP parameters affect both no-touch capacitance C_m, and the changes in capacitance for the two active touch states; $\Delta C'_\mathrm{m}$ for grounded and ΔC^*_m for ungrounded touch. From the graph of the Rx width sweep, we see that the parameter has different optimum values for maximizing $\Delta C'_\mathrm{m}$ or ΔC^*_m for the different electrode configurations. Depending on whether the TSP controller front end compensates for C_m, we should also consider that C_m increases with Rx width and reduces the relative capacitance change for higher Rx width. Also, increasing C_m will increase the amount of charged transferred on each charge transfer cycle, and thus increase the overall power consumption if charging voltage, frequency and number of pulses are kept constant.

For the sweeps of glass parameters, reduced glass thickness and increased relative permittivity in general leads to increased sensitivity to both ungrounded and grounded touch. This is explained by increased coupling between the electrodes and the object on the TSP surface. For configurations (A) and (B), reduced glass thickness leads to a higher increase in sensitivity to ungrounded touch than to grounded touch. The glass parameters affect C_m considerably more for configuration (C) than for configurations (A) and (B), as it influences the parallel

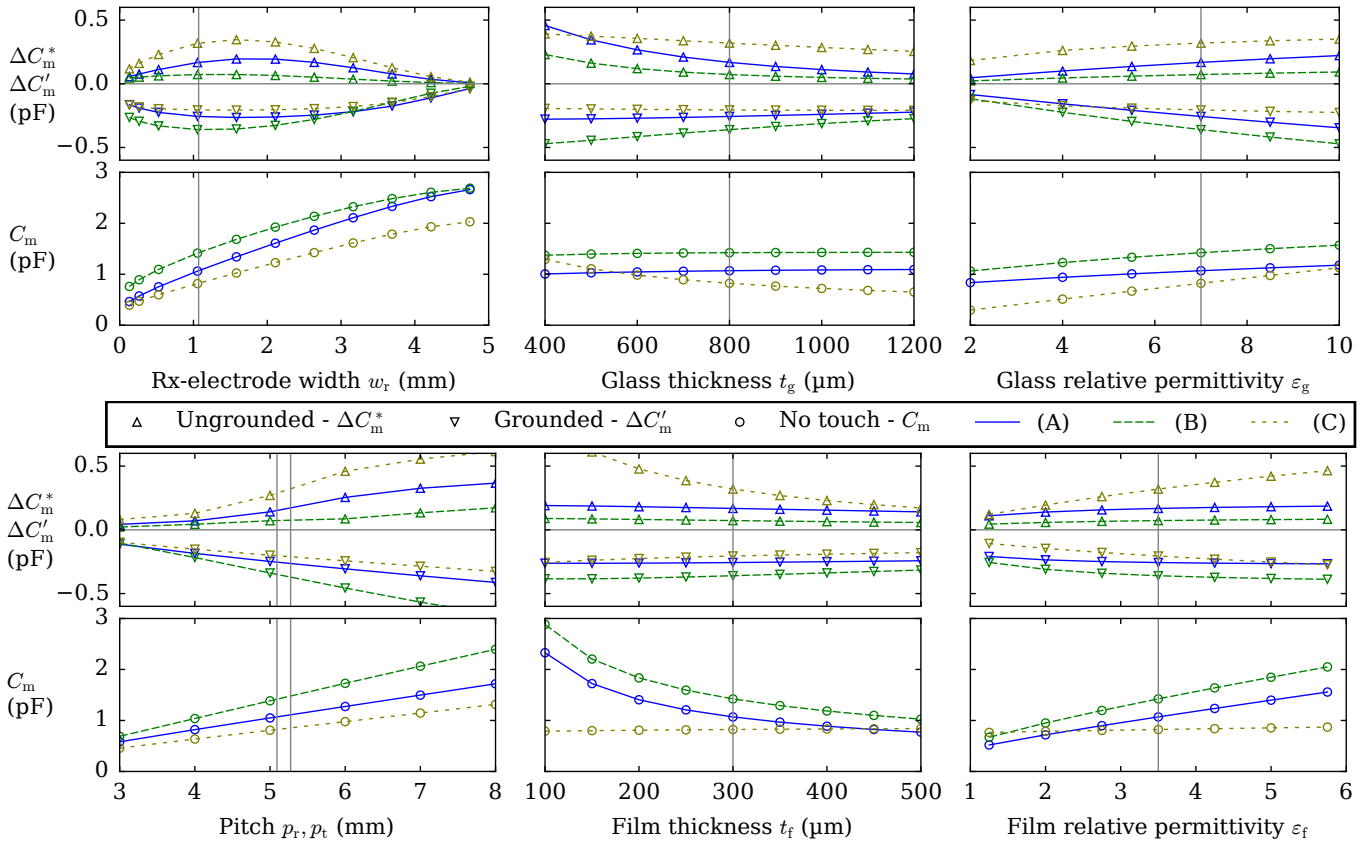

Fig. 7. Results of the parameter sweep for TSP parameters. The vertical lines mark the default values (different default values for p_t and p_r for pitch).

plate capacitance in the overlapping region of the Rx- and Tx-electrodes.

For the polymer film parameter sweeps, the roles are reversed for the two types of stack-ups, configurations (A) and (B) versus (C). This is to be expected, as the polymer film layer and glass layer are swapped in this case.

For the electrode pitch sweep, we see an increase in both C_m, $\Delta C_\mathrm{m}'$ and ΔC_m^* with increasing pitch. The overlap area between Tx-electrode and Rx-electrode increases almost linearly with the pitch, as the width of the Tx-electrode increases with pitch, while w_r is kept constant. This gives rise to nearly linear increase in C_m. The increase in magnitude of $\Delta C_\mathrm{m}'$ is also close to linear, resulting in an almost constant $\Delta C_\mathrm{m}'/C_\mathrm{m}$ for grounded touch. The increase in ΔC_m^* is however non-linear, resulting in a considerable increase of $\Delta C_\mathrm{m}^*/C_\mathrm{m}$ up to about $6\,\mathrm{mm}$, where also this value flattens out.

The results for the sweeps of the pad radius and the airgap between the TSP and the pad are shown in Fig. 8. In this case the C_m graphs are not included, as the pad does not influence the no-touch state. For the pad radius sweep, we see an increase in $\Delta C_\mathrm{m}'$ and ΔC_m^* up to about $4\,\mathrm{mm}$ radius. For this size the pad is covering the active intersection area completely and it is starting to overlap neighboring intersections. For configurations (A) and (C), there is a dip in $\Delta C_\mathrm{m}'$ for the sample at $6.5\,\mathrm{mm}$. This can be explained by the considerable increased overlap of the two neighboring Rx-electrodes at this size, leading to increased ground coupling, while at the same time no increased overlap with the active Tx-electrode. When the size grows further, this evens out.

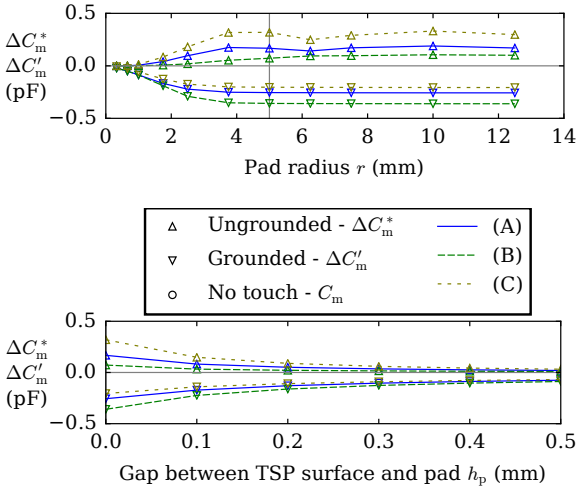

Fig. 8. Results of parameter sweep for pad parameters.

Regarding the air gap between TSP and pad, we see that both $\Delta C_\mathrm{m}'$ and ΔC_m^* falls off quickly as the gap increases up to about $0.1\,\mathrm{mm}$. $\Delta C_\mathrm{m}'$ however, does flattens out at a higher absolute value than ΔC_m^*, indicating that the TSP is less sensitive to ungrounded objects hovering over the screen

compared to grounded objects.

B. Pad Displacement

Fig. 9 shows the results for pad displacement for both grounded and ungrounded touch. For all cases of grounded touch, we see that $\Delta C'_{\mathrm{m}}$ is mainly dependent on the distance from the electrode intersection to the pad center. The transition in $\Delta C'_{\mathrm{m}}$ occurs as the perimeter of the pad moves across the active electrode intersection. Close examination reveals that the transition is slightly sharper in the y-direction for configurations (A) and (C). This is where the pad overlaps with the narrow Rx-electrode changes. As the Tx-electrodes are wider, the change in relative overlap is slower for displacement in x-direction. Since configuration (B) has double Rx-electrodes, there is less difference between the two directions here. This is of importance for the linearity of interpolating the touch center, where sharp transitions could lead to jagged diagonal motion.

For ungrounded touch, it is clearly not just a change of sign of ΔC_{m}. For all configurations we have a considerable positive ΔC^*_{m} when the pad is moved diagonally away from the electrode intersection into region 1 in Fig. 9. In this region, the pad is not overlapping the active intersection itself, however it is still overlapping both the Tx- and Rx-electrode of the intersection. This results in bridging of the electric field through the pad. For the area over the active intersection, the situation is as for no-touch. The net result is the observed increase in ΔC_{m}.

However, we also have regions of decreased capacitance, which are region 2 and 3 in Fig. 9. In these regions, the pad mainly overlaps one of the two intersecting active electrodes. The bridging effect is therefore not as strong as when the pad is centered on the active intersection. The pad also has a considerable overlap with inactive electrodes, resulting in capacitive coupling to ground. Except for region 2 in configuration (C), this results in a C_{m} lower than no-touch. We see that the shape of the image for configuration (C) is also different from that in (A) and (B). We explain this by the difference in the coupling between the pad and the two types of electrodes. As the pad and Rx-electrodes are only separated by a thin film in configuration (C), it has a stronger coupling between the Rx-electrode and the pad than in configurations (A) and (B).

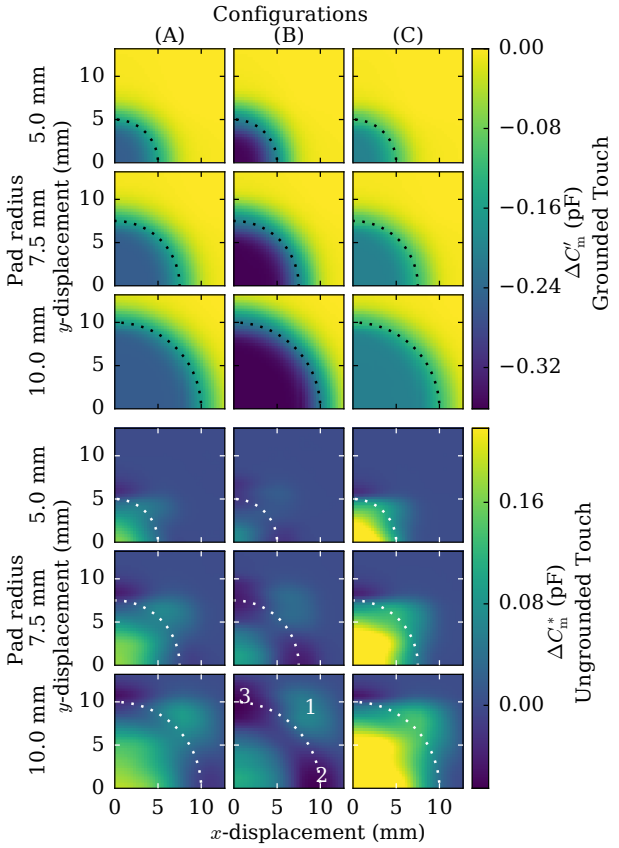

Fig. 9. FEM results for three different pad radii, showing $\Delta C'_{\mathrm{m}}$ and ΔC^*_{m} of an electrode intersection when the center of the pad is displaced relative to that electrode intersection in x- and y-direction. The Tx-electrodes are parallel to the y-axis. The dotted arc shows where the pad edge is above the electrode intersection. The numbers 1 to 3 mark regions of interest for the case of ungrounded touch.

C. Comparison With Experimental Data

By oscilloscope measurements of the Tx-signals in the GT-N8010, we found that it drives neighboring Tx-electrodes in pairs. This is with overlap, so each Tx-electrode is used twice during one complete scan cycle. We took this into account in the FEM simulations by including an extra Tx-electrode and letting C_{t} represent the capacitance between the pad and one active pair of Tx-electrodes in (4).

Fig. 10 shows the capacitance images for three different pad radii, both grounded and ungrounded, as sampled experimentally on the GT-N8010, along with the deviation of the corresponding FEM simulated capacitance images from the experimental results. The FEM simulations are for TSP configuration (A) with default parameters, as this model was based on the GT-N8010. To reduce noise, we repeated each measurement 4 times and averaged the pixel values. All of these measurements were made with the pad centered about the same touch pixel in the center of the TSP. As the pad is aligned to make the image symmetric about this pixel, we also averaged the results from all four quadrants. This leads to average of 4 samples for the center pixels, average of 8 samples for the 4 other pixels on the center axes and average of 16 samples for the 4 off center axes pixels. Deviations for the center pixel as well as Root Mean Square Deviation (RMSD) of pixels from one quadrant are listed in Table V. We note that the center pixel deviation is positive in all cases, indicating that the model shows a higher sensitivity to ungrounded than grounded touch as compared with the experiments. The largest deviations for ungrounded and grounded touch, those for the center pixels for the $7.5\,\mathrm{mm}$ pad, are both $11\,\%$ relative to respectively the maximum ΔC^*_{m} and the minimum $\Delta C'_{\mathrm{m}}$.

The samples from the GT-N8010 are acquired as raw integer counts from the TSP controller of unknown scale. For the comparison, we scaled the experimental data by a factor, $9.62 \times 10^{-16}\,\mathrm{F/count}$, found using a least squares fit with the corresponding simulation data. For the $10\,\mathrm{mm}$ radius pad,

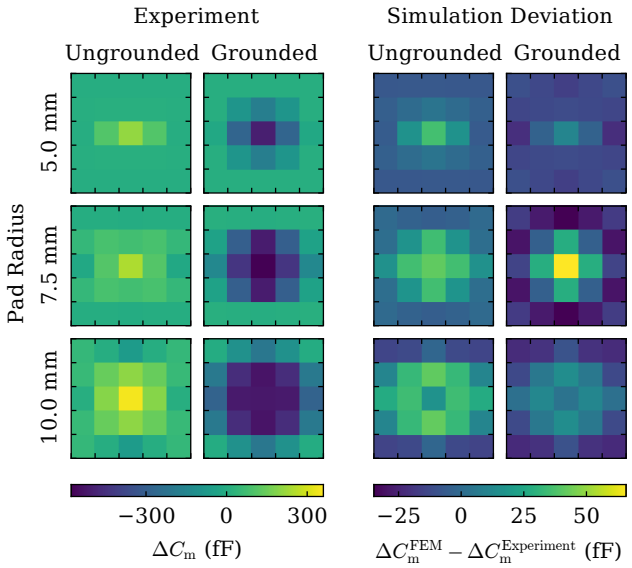

Fig. 10. Experimental results for ungrounded and grounded touch of pads of different radii for an area of 5 by 5 touch pixels. The raw values from the experiment have been scaled using a least square fit with the FEM results. Simulation deviation is the difference between the simulation results and the experimental results.

we can clearly see the reduction of ΔC_m orthogonal to the touch center in the ungrounded case, corresponding to regions 2 and 3 in Fig. 9. There is also a slight increase of ΔC_m in the corners, corresponding to region 1.

Touch sensitivity for TSPs may vary over the area of the panel. Towards the edges of the TSP, the capacitive couplings between electrodes and device ground may be different than in the middle of the TSP. To test the validity of the FEM results for pads close to the edges, we have therefore made measurements where the $7.5\,\mathrm{mm}$ pad is located in the corner of the TSP, so that it is centered on the 5 by 5 area of touch pixels in the corner. We made 3 measurements at each of the four corners. Comparing the average for each corner with the average from the center, we found a root mean square value of the differences of $5.6\,\mathrm{fF}$ for ungrounded and $12\,\mathrm{fF}$ for grounded touch. This variation in output for different areas of the screen is smaller than the corresponding RMSD values of the simulation, and we therefore expect the simulation results to be applicable as long as the capacitance image of the pad is within the screen area.

Possible sources of error apart from inaccuracies in the screen model parameters and noise in the experimental data include the geometry error due to the grounding of the pad and to a plastic ruler used to hold the ungrounded pads in place increasing the permittivity of the space around the pad.

D. Considerations For Ungrounded TUI Design

For a pad to be detected reliably by the TSP, it must generate a signal above the detection threshold on at least one electrode intersection no matter where on the TSP it is placed. This is satisfied if the capacitance change is above the detection threshold for all displacements up to $1/2$ pitch independently

TABLE V
FEM VS EXPERIMENT COMPARISON

	Pad radius (mm)	Center deviation[a](fF)	RMSD[b](fF)
Ungrounded	5.0	36	14
	7.5	41	23
	10	17	25
Grounded	5.0	11	13
	7.5	66	32
	10	3.3	13

[a] Experimental data subtracted from simulation data at the center pixel.
[b] Root Mean Square Deviation - the root mean square value of the deviation for each pixel in one quadrant of 3 by 3 pixels.

in x- and y-direction in Fig. 9. We see that the transition in ΔC_m occurs at lower displacements for ungrounded than for grounded touch. This, and the lower sensitivity to ungrounded touch especially for configuration (B), increases the minimum pad size required for ungrounded touch compared to grounded touch. Furthermore, interpolation of the ungrounded touch center is made more difficult by the irregular shape of the capacitance image. Hence a different interpolation algorithm will be needed for accurate determination of the pad center of a circular pad. With a considerable difference in the shape between the three different configurations, this interpolation algorithm will need to be tuned with respect to the TSP configuration.

In our simulations and experiments, we have only studied the effect of a single ungrounded pad. For a TUI application, several pads will be needed to identify the tangible and its state. Further work is therefore needed to see how TSP parameters, pad size and pad spacing influence the TSP output for multiple pads in close proximity. However some observations can be made from our simulations of single pads. As circular ungrounded pads affect the capacitance image within a square aligned with the TSP electrodes, of side length slightly larger than the pad diameter, they may require larger separation than grounded pads. In Fig. 9, if we for the $10\,\mathrm{mm}$ pad had a second pad displaced diagonally $20\,\mathrm{mm}$ in each direction relative to the first, then both pads would influence region 1. This makes it more difficult to interpret the capacitance image correctly as compared to the case of the pads being grounded.

V. FUTURE WORK

In order to speed up the development of ungrounded tangibles, it would be beneficial to develop a faster simulation tool. We propose doing this by estimating the capacitance matrix as a function of intersection area covered by the pad. FEM simulations can be used to find the capacitance per area for different touch conditions that would be needed as input parameters for such a model. A further step would be to develop and test untouched TUI objects on an actual TSP and to implement interpolation algorithms to handle the different shapes of the touch image of these TUI objects.

VI. CONCLUSION

By simulations and experiment, we have demonstrated the increase of the mutual capacitance reading output of a TSP

when an ungrounded conductive object is placed on its surface. This effect could be used to detect the presence of untouched TUI objects on mutual capacitance TSPs. The shape and size of the capacitance image of an ungrounded pad is different to that of a grounded pad, and it will therefore require different processing. In simulations, we found the TSP stack-up and the electrode configuration to have a considerable effect on the ratio of sensitivity to ungrounded versus grounded touch, with single Rx-electrodes in film-glass-film stack-up being 1.55 times more sensitive to ungrounded than grounded touch, whereas the sensitivity to ungrounded touch for double Rx-electrodes in glass-film stack-up is only 0.20 of that for grounded touch. We also found the TSP parameters to have different effect on the relative sensitivities. The relative sensitivity to ungrounded versus grounded touch can be increased by reducing the thickness and increasing the permittivity of the top layer of the TSP. It is also strongly influenced by the electrode pitch.

REFERENCES

[1] S. Jordà, G. Geiger, M. Alonso, and M. Kaltenbrunner, "The reacTable: Exploring the synergy between live music performance and tabletop tangible interfaces," in *Proc. TEI '07*, Baton Rouge, LA: ACM, 2007, pp. 139–146.

[2] M. Weiss, J. Wagner, Y. Jansen, R. Jennings, R. Khoshabeh, J. D. Hollan, and J. Borchers, "SLAP widgets: Bridging the gap between virtual and physical controls on tabletops," in *Proc. CHI '09*, Boston, MA: ACM, 2009, pp. 481–490.

[3] G. Barrett and R. Omote, "Projected-capacitive touch technology," *Inform. Display*, vol. 26, no. 3, pp. 16–21, 2010.

[4] J. Rekimoto, "SmartSkin: An infrastructure for freehand manipulation on interactive surfaces," in *Proc. CHI '02*, Minneapolis, MN: ACM, 2002, pp. 113–120.

[5] A. Wiethoff, H. Schneider, M. Rohs, A. Butz, and S. Greenberg, "Sketch-a-tui: Low cost prototyping of tangible interactions using cardboard and conductive ink," in *Proc. TEI '12*, Kingston, ON, Canada: ACM, 2012, pp. 309–312.

[6] T. Götzelmann and D. Schneider, "CapCodes: Capacitive 3D printable identification and on-screen tracking for tangible interaction," in *Proc. NordiCHI '16*, Gothenburg, Sweden: ACM, 2016, 32:1–32:4.

[7] N. H. Yu, L. W. Chan, S. Y. Lau, S. S. Tsai, I. Hsiao, D. J. Tsai, F. I. Hsiao, L. P. Cheng, M. Chen, and P. Huang, "TUIC: Enabling tangible interaction on capacitive multi-touch displays," in *Proc. CHI '11*, Vancouver, BC, Canada: ACM, 2011, pp. 2995–3004.

[8] S. Voelker, K. Nakajima, C. Thoresen, Y. Itoh, K. I. Øvergård, and J. Borchers, "PUCs: Detecting transparent, passive untouched capacitive widgets on unmodified multi-touch displays," in *Proc. ITS '15*, St. Andrews, Scotland: ACM, 2013, pp. 101–104.

[9] C. Holz, S. Buthpitiya, and M. Knaust, "Bodyprint: Biometric user identification on mobile devices using the capacitive touchscreen to scan body parts," en, in *Proc. CHI '15*, Seoul, South Korea: ACM, 2015, pp. 3011–3014.

[10] C. Honrado and T. Dong, "A capacitive touch screen sensor for detection of urinary tract infections in portable biomedical devices," *MDPI Sensors*, vol. 14, no. 8, pp. 13 851–13 862, Jul. 2014.

[11] L. Neamt, M. Bartis, and O. Chiver, "Capacitive touch sensors sensibility for different ground hatch and shield electrode structures," in *Proc. ATEE'2015*, Bucharest, Romania: IEEE, 2015, pp. 957–960.

[12] C. Thoresen, U. Hanke, and K. Øvergård, "Detection of ungrounded objects on mutual capacitance touch screens," in *Proc. 2015 IEEE SENSORS*, Busan, South Korea: IEEE, Nov. 2015, pp. 1–4.

[13] *Corning Gorilla Glass 5 PI sheet*, Rev. A, Corning Incorporated, Corning, NY, Jul. 2016.

[14] H. S. Kim and K. Y. Han, "High-SNR capacitive multi-touch sensing technique for AMOLED display panels," *IEEE Sensors J.*, vol. 16, no. 4, pp. 859–860, Feb. 2016.

[15] *Elmer*, CSC - IT Center for Science, Espoo, Finland. [Online]. Available: https://www.csc.fi/web/elmer (visited on Jan. 30, 2017).

[16] C. Geuzaine and J.-F. Remacle, "Gmsh: A 3-D finite element mesh generator with built-in pre-and post-processing facilities," *Int. J. for Numerical Methods in Eng.*, vol. 79, no. 11, pp. 1309–1331, 2009.

[17] S. Gevorgian and H. Berg, "Line capacitance and impedance of coplanar-strip waveguides on substrates with multiple dielectric layers," in *Proc. 31st European Microwave Conf.*, London, England, Sep. 2001.

[18] B. Cabral and L. C. Leedom, "Imaging vector fields using line integral convolution," in *Proc. SIGGRAPH '93*, Anaheim, CA: ACM, 1993, pp. 263–270.

Christian Bjørge Thoresen received the B.Sc. degree in electrical engineering from the University College of Southeast Norway (USN), Kongsberg, in 2008 and the M.Sc. degree in Microsystems technology from USN, Horten, in 2012. He is currently pursuing the Ph.D. degree at USN, Horten. His current interest of research is tangible user interface for capacitive touch screens.

Ulrik Hanke (SM'06) received the Siv.Ing. degree and the Dr.Ing. degree in physics from the Norwegian University of Science and Technology (NTNU), Trondheim, Norway, in 1989 and 1994, respectively. After two year as a Post. Doc. he worked for a decade as a research scientist at department of communication technology, SINTEF. Since 2006, he has been with University College of Southeast Norway, Horten, where he is a Professor of Micro- and Nanosystem technology. His current main research interest is in theory, design, and modeling of piezoelectric and RF acoustic micro devices.